# Steady RANS modelling of transitional ventilation room air flow

Steady RANS modelling of transitional ventilation room air flow

*Twan Van Hooff [1,2], Bert Blocken [1], GertJan van Heijst [3]*
*Eindhoven University of Technology Division of Building Physics, Katholieke Universiteit Leuven Fluid Dynamics Laboratory, Eindhoven University of Technology*

**SUMMARY**
Forced mixing ventilation is a commonly used ventilation principle in which air is forced into the upper part of the room at relatively high speeds. Attachment of the wall jet to the ceiling, also known as the 'Coanda effect', is used to ensure the air does not enter the occupant zone too early, thus preventing discomfort of the room occupants. Most mixing ventilation studies in the past have been conducted for wall jets with slot Reynolds numbers ($Re_{slot}$) that are considered to be in the turbulent regime, while a transitional flow regime can be present for low $Re_{slot}$ values. However, previous Computational Fluid Dynamics (CFD) studies have indicated possible deficiencies of the commonly used Reynolds-Averaged Navier-Stokes (RANS) equations in combination with a turbulence model to provide closure, when applied for transitional flows.
This paper presents a numerical analysis of forced mixing ventilation at a transitional slot Reynolds number ($Re_{slot} \approx 1{,}000$). CFD simulations of transitional wall jets in a confined space are conducted, using steady-state RANS modelling with difference turbulence models to provide closure. The results of the RANS simulations are compared with Particle Image Velocimetry (PIV) measurements in a reduced-scale model to assess the capability of the models to predict the transitional flow pattern. In addition, the ventilation efficiency is determined, demonstrating differences up to 36% in the calculated air exchange efficiency using different turbulence models.

**KEYWORDS**
*CFD simulations, PIV measurements, ventilation efficiency, forced mixing ventilation, reduced-scale model*

## 1 INTRODUCTION

The accurate prediction of ventilation flow is very important for a healthy, comfortable, sustainable and energy efficient indoor climate in buildings, airplanes, cars, etc., by removing pollutants, excess heat and moisture and, in extreme cases, fire, smoke and biochemical species. To quantify the effectiveness of the ventilation flow one can use the air exchange efficiency (Etheridge and Sandberg, 1996). The air exchange efficiency of an enclosure can be assessed by full-scale or reduced-scale experiments or by numerical simulation. The vast majority of building ventilation studies in the past has focused on slot Reynolds numbers ($Re_{slot}$) that are considered to be within the turbulent regime, with $Re_{slot}$ generally larger than 3,500 (e.g. Nielsen, 1974; Chen, 1995; Zhang and Chen, 2000). The slot Reynolds number can be defined as $Re_{slot} = (Uh)/\nu$ with U the characteristic inlet velocity in m/s, h the slot height in m and $\nu$ the kinematic viscosity ($m^2/s$). Transitional flow can be present inside a room for lower slot Reynolds numbers and exhibits flow features such as the shedding of coherent structures. This paper presents a comparison between 3D steady Computational Fluid Dynamics (CFD) simulations and reduced-scale Particle Image Velocimetry (PIV) measurements and of forced mixing ventilation driven by a transitional wall jet. The results obtained with several turbulence models are compared with the PIV measurements after which the differences in predicted air exchange efficiency are presented.

## 2 EXPERIMENTAL SET-UP

A reduced-scale setup has been built to perform flow visualisations and PIV measurements (Fig. 1). The setup consists of (1) a water column to drive the flow; (2) a flow conditioning section; (3) a cubic test section; and (4) an overflow. The conditioning section is placed in front of the inlet and consists of one honeycomb, three screens and a contraction to obtain a uniform water flow at the inlet and to minimize the turbulence level. The test section with edges of 0.3 m (L) is constructed from glass plates with a thickness of 8 mm. The slot inlet width (w) is 0.3 m (w/L = 1) and the height (h) can be varied up to 0.03 m ($0 < h/L \leq 0.1$); for this study h/L is fixed to 0.1. The height of the outlet is fixed at $h_{outlet}/L = 0.0167$. The 2 m high rectangular construction containing the water column is provided with inlet openings every 0.146 m to be able to vary the static pressure imposed by the water column. Inside the water column a screen has been added to limit the turbulence due to the insertion of the return water. The overflow behind the test section is fitted with a block that contains two STAD TA20 balancing valves (Fig. 1), enabling a step-wise adjustment of the volume flow rate through the test section.

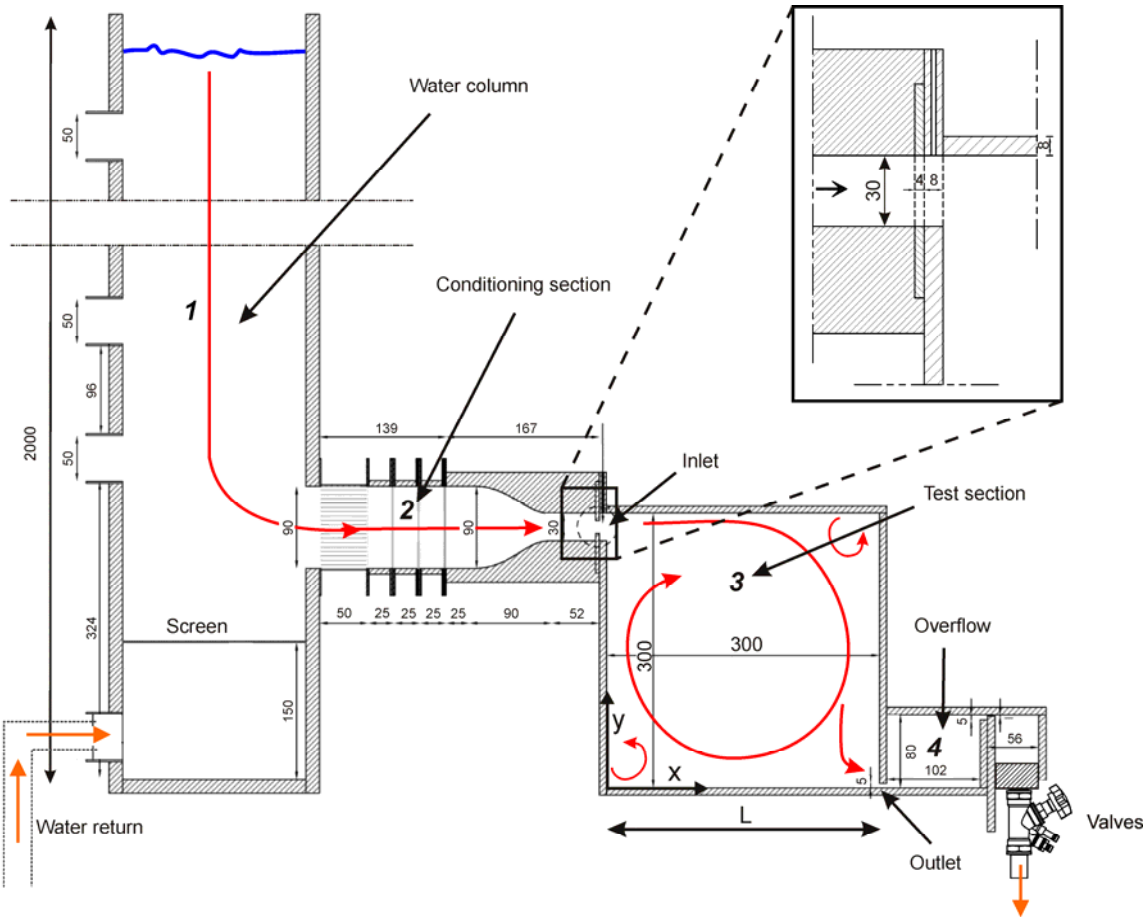


Figure 1. Reduced-scale setup used for flow visualizations and PIV measurements. This figure shows the water column (1), the flow conditioning section in front of the inlet (2), the test section (3), the overflow (4), and the valves that are placed in a block after the overflow. Dimensions in mm.

## 3 PIV MEASUREMENTS

The PIV measurements were conducted using a 2D PIV system consisting of a Nd:Yag (532 nm) double-cavity laser (2 x 200 mJ, repetition rate < 10Hz) used to illuminate the field of view, and one CCD (Charge Coupled Device) camera (1376 x 1040 pixel resolution, 10 frames/s) for image acquisition. The laser was mounted on a translation stage; the camera was positioned perpendicular to the water cube. Seeding of the water was provided by hollow

glass micro spheres (3M; type K1) with diameters in the range of 30 – 115 μm. Image acquisition and post-processing was performed with the software package Davis 7.1 (LaVision). The measuring frequency had to be sufficiently low to obtain statistically-independent (uncorrelated) samples (i.e. velocity vector fields) in order to determine time-averaged flow quantities. The required measuring frequency was calculated from the integral length scale and the characteristic velocity and was set to 1.67 Hz. Each measurement set consisted of 360 uncorrelated samples. The time-averaged velocity fields were obtained by averaging the 360 instantaneous velocity vector fields.
Based on flow visualizations, PIV measurements were conducted for an inlet height h/L = 0.1 and $Re_{slot}$ ranging from 300 to 2,500. For brevity, only the results for $Re_{slot} \approx 1{,}000$ are shown in this paper. Two sets of PIV measurements were performed in the vertical centre plane (z/L = 0.5) of the water cube. The first set of measurements consists of data in the entire cross-section of the cube, i.e. a flow field of 0.3 x 0.3 $m^2$. The second set contains PIV measurements in a smaller area in the proximity of the inlet, enabling a higher measurement resolution of the wall jet.

## 4 CFD SIMULATIONS: COMPUTATIONAL MODEL AND PARAMETERS

The dimensions of the computational model of the test section and the contraction are identical to the dimensions of the water cube that has been used for the flow visualisations and the PIV measurements (Fig. 2a). The computational grid is fully structured (Fig. 2b) and is made using the grid-generation technique described by van Hooff and Blocken (2010). The grid resolution is increased in areas of expected large velocity gradients, e.g. the interference between the jet and the ambient flow and the boundary layer flow at the top surface of the cube. A grid-sensitivity analysis is performed to assess the grid convergence using five grids, based on a linear grid refinement factor of √2. The grid-sensitivity analysis indicated that the results can be considered to be fairly grid independent from Grid 4 onwards. The CFD simulations are therefore conducted with a 1,203,200 cells grid.

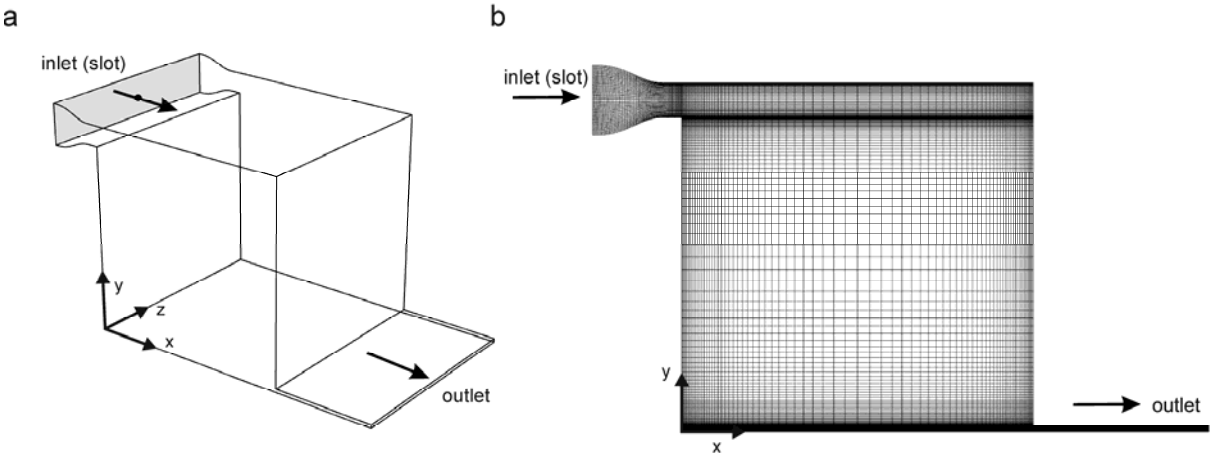


Figure 2. (a) Computational model of the water cube. (b) Computational grid used for the CFD simulations (1,203,200 cells).

A constant velocity is imposed at the inlet, based on $Re_{slot}$ and the measured velocity using the 2D PIV system. Turbulence properties are included by defining the time-averaged turbulence intensity $I = R_{RMS}/R_M = 6\%$, with $R_M$ the maximum velocity magnitude, and a hydraulic diameter ($L_h = 0.0545$ m). Zero static pressure is set at the outlet of the domain. The top, bottom and side walls are modelled as no-slip walls.
The 3D steady RANS equations are solved in combination with four different turbulence models; RNG k-ε (Yakhot et al., 1992), SST k-ω (Menter, 1994), low-Re k-ε (Chang et al.,

1995), and RSM low-Re stress-omega model (Wilcox, 1998), using the commercial CFD code Fluent 6.3.26 (Fluent Inc., 2006). Low-Reynolds number modelling (LRNM) is used to solve the flow all the way down to the wall, including the thin laminar sublayer. In order to use LRNM the grid resolution near the wall has to be sufficiently small, i.e. the $y^*$ value in the wall-adjacent cell should be lower than $y^* = 5$, and preferably around $y^* \approx 1$. The $y^*$ value for Grid 4 is sufficiently small for LRNM ($y^* \approx 1$). Pressure-velocity coupling is taken care of by the SIMPLE algorithm, pressure interpolation is second order, and second order discretisation schemes are used for both the convection terms and the viscous terms of the governing equations. The simulations were terminated when additional iterations showed no further convergence.

## 5 CFD VALIDATION AND RESULTS

The results of the PIV measurements for $Re_{slot} \approx 1{,}000$ are compared with the results of the CFD simulations with the four different turbulence models. The comparison is made using the dimensionless x-velocity ($U/U_M$) on two vertical lines in the centre plane ($z/L = 0.5$) at $x/L = 0.5$ (Fig. 3a), and $x/L = 0.8$ (Fig. 3b), respectively. Note that the dimensionless x-velocity $U/U_M$ is used instead of the dimensionless velocity magnitude $R/R_M$, in order to be able to illustrate the streamwise flow direction in the water cube. Figure 3 indicates that the results obtained with the RNG k-ε model are quite poor; the separation of the wall jet from the top is not predicted accurately. This inadequacy of the RNG k-ε model is caused by the inability of the high-Reynolds number k-ε models to predict boundary layer flows with an adverse pressure gradient. The results of the other three models are in closer agreement with the measurement results; the best overall agreement is obtained with the RSM model, at least for these two profiles and for this particular set-up with of $h/L = 0.1$ and $Re_{slot} \approx 1{,}000$.

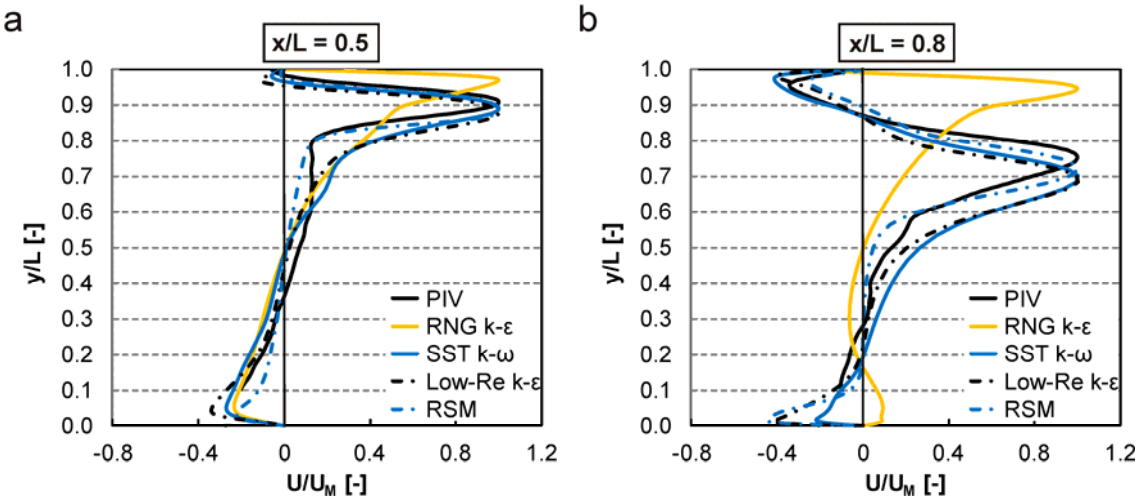


Figure 3. Comparison PIV measurements with numerical results. (a) $x/L = 0.5$; (b) $x/L = 0.8$.

The influence of the turbulence model on the calculation of the air exchange efficiency is assessed. The air exchange efficiency $\varepsilon_a$ is defined as with $\tau_n$ the nominal time constant, which is the shortest possible time it takes to replace the air, and $\bar{\tau}$ the volume average age of air (Etheridge and Sandberg, 1996). In the case of perfect mixing the air exchange efficiency would be equal to 0.5, since the average age of air in the room would in this case be equal to the age of air at the exhaust (= nominal time constant). By solving a transport equation for a passive scalar in CFD it is possible to numerically determine the age of air inside the enclosure, enabling the calculation of the air exchange efficiency using CFD (e.g. Chanteloup and Mirade, 2009). Figure 4 shows contours of the age of $\varepsilon_a = \tau_n / 2\bar{\tau}$ air in the cube, obtained with the four different turbulence models. Due to the deviations in flow field, the

calculated air exchange efficiency obtained with the RNG k-ε model, 0.45, differs considerably from the values of $\varepsilon_a$ obtained with the SST (0.37), low-Re k-ε (0.37) and the RSM model (0.33). The largest difference is present between the RNG k-ε model and the RSM model, which is 36%.

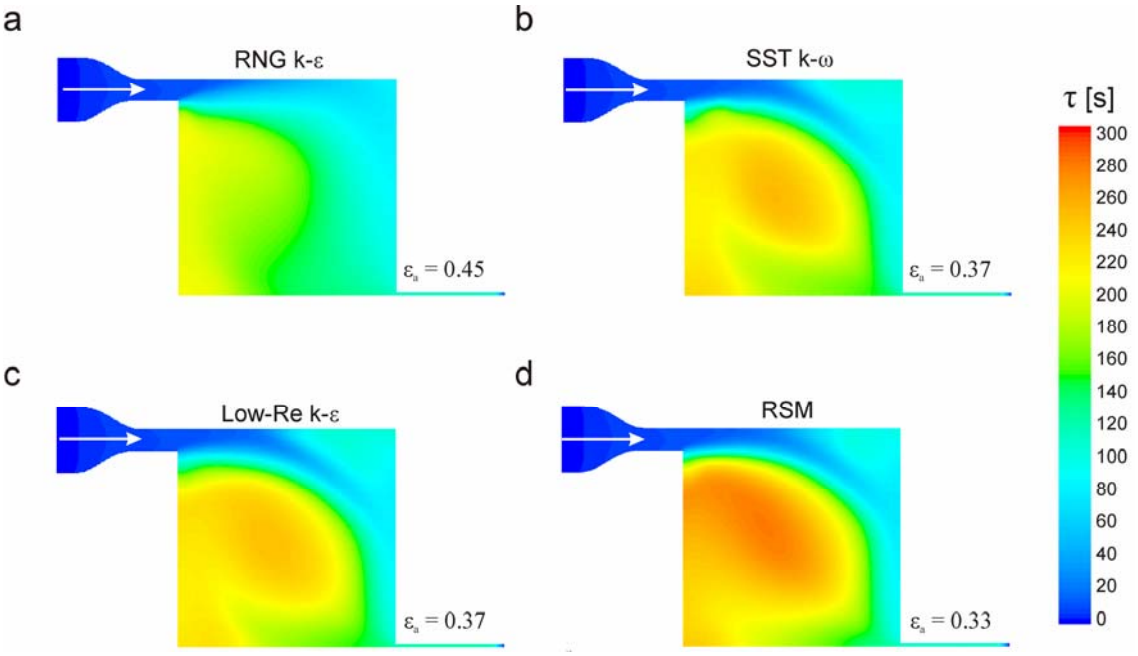


Figure 4. Computed age of air in the set-up. (a) RNG k-ε model; (b) SST k-ω model; (c) low-Re k-ε model; (d) RSM low-Re stress-omega model.

## 7 DISCUSSION

This paper presents some first results of a study on forced mixing ventilation at transitional slot Reynolds numbers. Future work will include a more extensive validation of numerical models for a range of $Re_{slot}$ values and other inlet heights. The influence of cell size and turbulence intensity on the flow pattern and the point of separation will be studied in more detail. Furthermore, additional RANS turbulence models, as well as Large Eddy Simulation will be tested.

## 8 CONCLUSIONS

This paper reports on 3D steady RANS CFD simulations of forced mixing ventilation driven by a transitional wall jet ($Re_{slot} \approx 1{,}000$). The CFD simulations were validated using PIV measurements that were conducted in a reduced-scale experimental setup. The visualisations have shown that the flow is transitional for a slot height h/L = 0.1 and for this value of $Re_{slot}$. The CFD simulations were conducted with four different turbulence models (RNG k-ε, SST k-ω, Low-Re k-ε and a RSM model). The flow pattern obtained with the RNG k-ε turbulence model showed large deviations with the measured flow pattern due to the inability of this model to predict the flow separation due to the adverse pressure gradient. The results for the three other models showed a fair to good agreement with the measurement results. In general, the results obtained with the RSM model showed the best agreement for this specific case. As a result of the differences in predicted flow pattern the results for the calculated air exchange efficiency showed a relatively large difference between the RNG k-ε model on the one hand, and the SST k-ω, Low-Re k-ε and RSM models on the other hand. For example, the difference between the RNG k-ε model and the RSM model is 36%. This study illustrates the large differences that can be present when performing the same study with different turbulence models. Caution should be taken in the process of choosing the computational

methods and models to avoid erroneous ventilation predictions. Additional comparative studies are needed to evaluate the validity of the present findings beyond the single slot height (h/L = 0.1), $Re_{slot}$ and slot geometry investigated here, and to test other computational parameters that might influence the predicted flow pattern.

## 10 REFERENCES


Chen Q. 1995. Comparison of different k-ε models for indoor air flow computations, *Numerical Heat Transfer Part B: Fundamentals*, 28, 353-369.

Chang K.C., Hsieh W.D., Chen C.S. 1995. A modified low-Reynolds-number turbulence model applicable to recirculating flow in pipe expansion. *Transactions of the ASME, Journal of Fluids Engineering*, 117, 417–423.

Chanteloup V. and Mirade P.S. 2009. Computation fluid dynamics (CFD) modeling of local mean age distribution in forced food plants. *Journal of Food Engineering*, 90, 90–103.

Etheridge D.W. and Sandberg M. 1996. *Building Ventilation: Theory and Measurement*. London: Wiley; 1996.

Fluent Inc. 2006. Fluent 6.3 user's guide, Lebanon.

Menter F.R. 1994. Two-equation eddy-viscosity turbulence models for engineering applications, *AIAA Journal*, 32(8), 1598-1605.

Nielsen P.V. 1974. *Flow in air conditioned rooms (model experiments and solution of the flow equation)*. PhD Thesis, Danish Technical University, Copenhagen

Nielsen P.V. 1998. The selection of turbulence models for prediction of room airflow, *ASHRAE Transactions*, 104(1B), 1119-1127.

van Hooff T. and Blocken B. 2010a. Coupled urban wind flow and indoor natural ventilation modelling on a high-resolution grid: A case study for the Amsterdam ArenA stadium. *Environmental Modelling & Software*, 25, 51-65.

Wilcox D.C. 1998. Turbulence modeling for CFD. DCW Industries Inc., La Canada, California, USA.

Yakhot V., Orszag S.A., Thangam S., Gatski T.B., Speziale C.G., 1992. Development of turbulence models for shear flows by a double expansion technique. *Physics of Fluids A*, 4, 1510-1520.

Zhang W. and Chen Q. 2000. Large Eddy Simulation of indoor airflow with a filtered dynamic subgrid scale model. *International Journal of Heat and Mass Transfer*, 43, 3219–3231.